International Journal of Control Theory and Applications

ISSN : 0974-5572

Volume 10 • Number 35 • 2017

Lung Parenchyma Detection using Levelset Segmentation

K. Murali Krishna[a], Md. Zia Ur Rahman[b], B. Sowjanya Lakshmi[c], Ch. Padma Priya[d], A. Blessy[e] and M. Thirumala Gayathri[f]

[a-f]Department of E.C.E., KKR & KSR Institute of Technology & Sciences, Vinjanampadu, Guntur, A.P, India. Email: [a]muralikondaveeti1@gmail.com; [b]mdzr55@gmail.com

Abstract: In real world images the most considered challenge in image segmentation is intensity inhomogenity. Out of algorithms of image segmentation, region based algorithm is applied only for the homogeneity of images which does not provide accurate segmentation results for intensity inhomogenity. To deal with intensity inhomogenity of images, a novel region-based method is proposed in this paper. Firstly, based on the intensity inhomogenity of the image models, clustering property of local intensities of the image intensities is derived and a criterion function of local clustering for the image intensities in the neighborhood of each point is defined. The global criterion of image segmentation can be obtained by integrating the local clustering criterion function with respect to the neighborhood center. This global criterion defines in energy in terms of level set functions, in a level set formulation that represents partition of the image domain in the bias field that accounts for the intensity inhomogenity of the image. This method is able to together segment the image and estimate the bias field by minimizing this energy. This estimated bias field can be used for intensity inhomogenity correction. **This method has been used for segmentation and bias correction of magnetic resonance (MR) images with promising results.**

Keywords: Bias field, Inhomogenity, Intensity, Level-set, Segmentation.

1. INTRODUCTION

Automated lung segmentation on chest **magnetic resonance (MR) images** is critical for efficient computer-aided diagnosis (CAD) of pulmonary diseases [17-21]. Unfortunately, the huge range of images and diagnostic measurements for different lung pathologies make correct, fast, and low cost segmentation a challenge. For instance, pathology-related segmentation failures lose important data, being needed for studying radiation pneumonitis development. Intensity inhomogenity typically occurs in real-world images due to many reasons, such as illumination spatial variations and of imaging devices with imperfections, which raises many difficulties in image processing and computer vision. For the intensity inhomogenity images the image segmentation is difficult because of the overlaps among the intensity ranges in the segmented regions. So it is difficult to identify these regions based on the intensity value of the pixel. There are widely used image segmentation algorithms

[1-4] based on intensity homogeneity, and are not valid for intensity inhomogenity images. Generally in image segmentation intensity inhomogenity is difficult.

Actually the level set method is used as numerical technique for interfaces and shapes tracking. In level set method, the surfaces are depicted as zero level set of the higher order dimensional function called, level set parameter. The segmentation problem can be solved with this level set method. The level set method is generally categorized into two classes: region based models [10-14] and edge-based models [5-7]. In region-based model it just identifies the region of interest using region descriptor. But it is difficult to define the region descriptor for the intensity inhomogenity images. Almost all the region-based models [8] are based on intensity homogeneity. In a novel region-based method [9], local intensity clustering property property is derived.

In this paper, we propose a novel region-based method for lung image segmentation. From a generally accepted model of images with intensity inhomogeneities, we derive a local intensity clustering property, and therefore define a local clustering criterion function for the intensities in a neighborhood of each point. This local clustering criterion is integrated over the neighborhood center to define an energy functional, which is converted to a level set formulation. Minimization of this energy is achieved by an interleaved process of level set evolution and estimation of the bias field. As an important application, our method can be used for segmentation and bias correction of magnetic resonance (MR) lung images.

2. LEVEL SET FORMULATIONS AND ENERGY MINIMIZATION

We expressed the proposed energy P_E in terms of the regions $\phi_1, \ldots, \phi_N$. To derive the solution for the energy minimization problem from the expression P_E is difficult. By representing the proposed energy P_E in terms disjoint regions $\phi_1, \ldots, \phi_N$ with number of level set functions ,with a regularization term on these level set functions can be converted into level set formulation. By using well-established variation methods in the level set formulation we can solve the energy minimization problem.

Level set function is a function which is used to represent a partition of the domain ϕ into two disjoint regions $\phi_1, \ldots, \phi_N$ by taking positive and negative signs.

Let Ω: ϕ –> Q be a level set function, then its signs define two disjoint regions

$$\Phi_1 = \{A : \Omega(A) > 0\}, \text{ and } \phi_2 = \{A: \Omega(A) < 0\} \tag{1}$$

Which form a partion of the domain ϕ. Two or more level set functions can be used to represent M regions $\phi_1,\ldots,\phi_N$ in the case M > 2. The level set formulation of the energy P_E

For the case of N = 2 and N = 2, called two-phase and multi phase formulations, respectively, will be given in the next two sub sections.

A. Two-phase Level Set Formulation

In this case The image domain ϕ is segmented into two disjoint regions $\phi_1, \ldots, \phi_N$. The regions $\phi_1, \ldots, \phi_N$ can be represented by their member functions $F_1(\Omega) = H(\Omega)$ and $F_2(\Omega) = 1 - H(\Omega)$, respectively, where H is Heaviside function. For M = 2, the energy can be expressed as the following level set formulation

$$P_E = \int \left(\sum_{x=1}^{M} \int N(B-A) \left| I(A) - y(B) z_x \right|^2 \right) F_x(W(a))\, da \tag{2}$$

By exchanging the order of integrations, we have

$$P_E = \int \left(\sum_{x=1}^{M} \int N(B-A) \left| I(A) - y(B) z_x \right|^2 db \right) F_x(W(a))\, da \tag{3}$$

For, the constants are represented as $z_1, \ldots, z_M$ with a vector $z = (z_1, \ldots, z_M)$. Thus the level set function Ω, the vector z, and the bias field y are the variables of the energy P_E, which can therefore be written as $P_E(\Omega, z, y)$. From (3) we can rewrite the energy $P_E(\Omega, z, y)$ in the following form:

$$P_E(\Omega, z, y) = \int \sum_{x=1}^{M} e_x\,(a) F_x(\Omega(a))da \tag{4}$$

where, e_x is the function given by

$$e_x(a) = \int N\,(b-a)\,|I(A) - y(b)z_x|^2 db \tag{5}$$

By using the equivalent expression the function e_i can be computed

$$e_i(a) = I^2 1_N - 2_{Zi} I(y \times N) + z_i^2 (y^2 \times N) \tag{6}$$

where * is convolution operation, and 1_N is the function defined by $1_N(A) = \int N(B-A)dB$ which is equal to constant 1 everywhere except near the boundary of the image domain Φ.

The above defined energy $P_E(\Omega, z, y)$ is used as the data term in the energy [15-19] of the proposed variational level set formulation which is defined by

$$L(\Omega, z, y) = P_E(\Omega, c, y) + ul(\Phi) + \mu P_R(\Omega) \tag{7}$$

Where $l(\Phi)$ and $P_R(\Omega)$ are the regularization terms. They are defined as follows

$$l(\Omega) = \int |\Delta H(\Omega)|\, da \tag{8}$$

which computes the length of the zero level counter of Ω and therefore serves to smooth the counter by penalizing its length. The energy term $P_R(\Phi)$ is defined by

$$P_R(\Omega) = \int R\left(|\Delta\Omega|\right) da \tag{9}$$

With a potential function $R:[0, \infty) \rightarrow O$ such that $R(n) \geq P_R(1)$ for all s. i.e, $s = 1$ is a minimum point of R. In this paper, we use the potential function R defined by $R(n) = (1/2)(s-1)^2$. Obviously, with such a potential R, the energy $P_R(\Omega)$ is minimized when $|\Delta\Omega| = 1$, which is the characteristic of a signed distance function, called the signed distance property. Therefore, the regularization term $P_R(\Omega)$ is called a distance regularization term, which was introduced by Li et. al., [10] in a more general variational level set formulation called distance regularized level set evolution (DRLSE) formulation. Observe the equation [11] for the necessity and the mechanism of maintaining the signed distance property of the level set function in DRLSE.

We can obtain the result of image segmentation given by the level set function Ω and the estimation bias field b by minimizing this energy. With the help of iterative process we can achieve the energy minimization: in each iteration, we can minimize the energy $L(\Omega, z, y)$ with respect to each of its variables Ω, z and y, given the other two updated in previous iteration. We give the solution to the energy minimization with respect to each variable as follows:

1. *Energy Minimization with Respect to* Ω*:* The minimization of $L(\Omega, z, y)$ with respect to Ω can be achieved by using standard gradient descent method, namely, solving the gradient [20] flow equation by fixing z and y

$$\frac{\partial \Omega}{\partial t} = -\frac{\partial L}{\partial \Omega} \tag{10}$$

where, $\partial L/\partial\Omega$ is the Gateaux derivative [1]of the energy L.

By calculus of variations [1], we can calculate the Gateaux derivative $\partial L/\partial \Omega$ and express the equivalent gradient flow equation as

$$\frac{\partial \Omega}{\partial t} = -\delta(\varnothing)(e_1 - e_2) + u\delta(\Omega)\mathrm{div}\left(\frac{\nabla \Omega}{\nabla \Omega}\right) + \mu\ \mathrm{div}(d_R(|\nabla \Omega|)\nabla \Omega) \tag{11}$$

where, ∇ is the gradient operator, div(.) is the divergence operator, and the function d_p is defined as

$$d_R(n) = \frac{R'(n)}{n} \tag{12}$$

during the evolution of level set function according to [12] the constants z_1 and z_2 in z and the bias field y are updated by minimizing the energy $P_E(\Omega, z, y)$ with respect to z and y, respectively, which are described below.

2. *Energy Minimization with Respect to z*: For fixed Ω and y, the optimal z that minimizes the energy $P_E(\Omega, z, y)$, denoted by $z = (z_x, \ldots, z_M)$ is given by:

$$v_x = \frac{\int (y \times N)\, Ivxd B}{\int (y2 \times N) vxd B}, x = 1, \ldots, M \tag{13}$$

with $v_x(B) = F_x(\Omega(B))$

3. *Energy minimization with respect to y*: For fixed Ω and z, the optimal y that minimizes the energy $P_E(\Omega, z, y)$, denoted by y, is given below

$$Y = \frac{IJ(1) \times N}{J(2) \times N} \tag{14}$$

where, $J(1) = \sum_{x=1}^{M} z_x v_x$ and $J(2) = \sum_{x=1}^{M} z_x^2 v_x$.

The convolutions with a kernel function N in (14) confirm the slowly varying property of the derived optimal estimator y of the bias field.

Multiphase Level Set Formulation

For the case of $M \geq 3$, we can use two or more level set functions $\Omega_1, \ldots, \Omega_k$ to define M membership functions F_x of the regions ϕ_x, $x = 1, \ldots, M$,

$$F_x(\Omega(B), \ldots, \Omega(B)) = \begin{cases} 1, B \in \phi x \\ 0, \text{else} \end{cases}$$

We use two level set functions Ω_1 and Ω_2, in the case $M = 2$ to define $F_1(\Omega_1, \Omega_2)H(\Omega_1)H(\Omega_2)$, $F_2 = (\Omega_1, \Omega_2) = H(\Omega_1)(1 - H(\Omega_2))$, and $F_3(\Omega_1, \Omega_2) = 1 - H(\Omega_1)$ to give a three phase level set formulation [21] of our method. For the four-phase case $M = 4$, the definition of F_x can be defined as $F_1(\Omega_1, \Omega_2) = H(\Omega_1)H(\Omega_2)$, $F_2(\Omega_1, \Omega_2) = H(\Omega_1)(1 - H(\Omega_2))$, $F_3(\Omega_1, \Omega_2) = (1 - H(\Omega_1))H(\Omega_2)$, and $F_4 = (1 - H(\Omega_1))(1 - H(\Omega_2))$.

For simple notation we denote these level set functions $\Omega_1, \ldots, \Omega_N$ by a vector valued functions $\Omega = (\Omega_1, \ldots, \Omega_N)$. Thus the membership function $F_x(\Omega_1(y), \ldots, \Omega_N(\phi))$ can be written as $F_x(\Omega)$. The energy P_E can be converted to multi phase level set formulation

$$P_E(\Omega, x, y) = \int \sum_{x=1}^{M} e_x(A) F_x(\Omega(A)) Da \tag{15}$$

The energy function L in our multi phase level set formulation is defined by

$$L(\Omega, z, y) = P_E(\Omega, z, y) + P_R(\Omega) \tag{16}$$

The minimization of energy $L(\Omega, z, y)$ in (16) with respect to the variable $\Omega = (\Omega_1, \ldots, \Omega_N)$, can be performed by solving the gradian flow equations:

$$\frac{\partial \Omega 1}{\partial t} = -\sum_{x=1}^{M} \frac{\partial FX(\Omega)}{\partial \Omega 1}\, e_x + u\delta(\Omega_1)\mathrm{div}\left(\frac{\nabla \Omega 1}{|\nabla \Omega 1|}\right) + \mu \mathrm{div}(d_R(|\nabla \Omega 1|\Delta\Omega_1)$$

$$\frac{\partial \Omega k}{\partial t} = -\sum_{x=1}^{M} \frac{\partial F_x(\Omega)}{\partial \Omega k}\, e_x + u\delta(\Omega_k)\mathrm{div}\left(\frac{\nabla \Omega k}{|\nabla \Omega k|}\right) + \mu\ \mathrm{div}(d_R(|\nabla \Omega_k|)\nabla \Omega_k). \tag{17}$$

The minimization of the energy $P_E(\Omega, z, y)$ can be achieved by the same procedure as in the two phase case. And this is easy to show that z and y that minimize the energy $P_E(\Omega, z, y)$ with $u_x = F_x(\Omega)$ for $x = 1, \ldots, N$.

C. Numerical Implementation

Our method is straightforwardly implemented by using the same finite difference scheme as for the DRLSE provided in $\{P_E\}$ the level set evolution can be implemented. To implement the proposed level set method we use easy full domain implementation, we can use the narrow band implementation of the DRLSE which would greatly reduce the computation cost and make the algorithm significantly faster than the full domain implementation.

The Heaviside function H is replaced by a smooth function that approximates H, called the smoothed Heaviside function H_ε, which is defined by

$$H_\varepsilon(X) = \frac{1}{2}\left[1 + \frac{2}{\pi}\arctan\left(\frac{X}{\epsilon}\right)\right] \tag{18}$$

where, $\varepsilon = 1$. Accordingly, the dirac delta function δ, which is derivative of Heaviside Function H, is repaced by derivative of $H\epsilon$, which is computed by

$$\delta_\varepsilon(X) = H'_\varepsilon(X) = \frac{1}{\pi}\frac{\epsilon}{e2 + X2} \tag{19}$$

At each and every step, the constant $z = (z_1, \ldots, z_M)$ and the bias field b are updated according to (13) and (14). With $v_x = F_x(\Omega)$.

The two convolutions $y \times N$ and $y^2 \times N$ for the computation of e_x also appear in the computation of e'_x for all $x = 1 \ldots N$. Another two convolutions $(IJ(1)) \times K$ and $J(2) \times K$ for the bias field y. Thus there are a total of four convolutions to be computed at each time step during the evolution of Ω. The convolution kernel K is constructed as a $w \times w$ mask, with w being the smallest odd number such that $w \geq 4 \times \alpha + 1$, when K is defined as the Gaussian kernel in P_E. For example, given a scale parameter $\alpha = 4$, the mask size is 16×16.

The parameters such as μ and the time step Δt, can be fixed as $\mu = 1.0$ and $\Delta t = 0.1$. Our model is not sensitive to the choice of the parameters. The parameter u is usually set to 0.001×255^2 as a default value for the most of digital images with intensity range in [0.225]. The parameter α and the size of the neighborhood O_b should be relatively smaller for images with more localized intensity in-homogeneties.

D. MR Image Segmentation and Bias Correction

The main focus of this subsection is to segmentation of the lung images as well as bias correction of those images. The first column of the Figure 1 shows the image to which results are obtained. These images display

clear intensity inhomogenities. The results of segmentation and estimated bias field and bias corrected images are observed in second, third and fourth column of the Figure 1 respectively. In bias corrected images, intensities become quite homogeneous which are within each tissue. The histograms of the bias corrected images and the original images are compared to demonstrate the improvement of the image quality in terms of intensity homogeneity. The histogram of original image is plotted in the fifth column and similarly histogram of the bias corrected image in the sixth column. In the histogram of the bias corrected image there are well separated peaks in which each corresponds to background in image. From comparison, it is clear that the histogram of original image does not have well separated peaks because of intensity distribution due to bias.

3. EXPERIMENTATION RESULTS

First we substantiate our method in the phase of two cases. In this section the parameter σ is set to five for this experiment. All the reaming parameters are set to the default values. The processes of curve evolutions are characterize by illustrate the left column has initial contours, the middle column has intermediate contours and finally the right column has the final contours. These two images can see clearly of intensity in homogeneities. The adorable segmentation result for such images by using in this method. The field of approximate bias '*b*' used for intensity in homogeneities correction by using this method. The given estimating bias field *b* the corrected bias image quotient $1/\hat{b}$. This method capability to prove the simultaneous segmentation and field estimation of bias. This method applied to the medical images. That is the *x*-ray image of lung shows the obvious intensity in homogeneities in these images. The ultrasound image is also corrupted with serious speckle noise. We applied a convolution with a Gaussian kernel to smooth the ultrasound image as a preprocessing step. The scale parameter of the Gaussian kernel is chosen as 2.0 for smoothing this ultrasound image. The initial contours are plotted on the original images in Figure 1(a). The corresponding results of segmentation, bias field estimation, and bias correction are shown in Figure 1(b), Figure 1(c), and Figure 1(d), respectively. These results demonstrate desirable performance of our method in segmentation and bias correction.

A. MR Image Segmentation and Bias Correction

In this paper we focus on the application of the proposed method to segmentation and bias correction of brain MR images. We show the results for MR image in Figure *s*(*a*). These images exhibit obvious intensity inhomogeneities. The segmentation results, computed bias fields, bias corrected images, are shown in Figure 2(b), Figure 2(d), and Figure 2(e) respectively. It can be seen that the intensities within each tissue become quite homogeneous in the bias corrected images. The improvement of the image quality in terms of intensity homogeneity can be also demonstrated by comparing the histograms of the original images and the bias corrected images. The histograms of the original images and the bias corrected images are plotted in Figure 2(f). There are three well-defined and well-separated peaks in the histograms of the bias corrected image, each corresponding to a tissue or the background in the image. In contrast, the histograms of the original images do not have such well-separated peaks due to the mixture of the intensity distribution caused by the bias.

4. CONCLUSION

We have presented a deviational framework of level set method for segmentation and bias correction of image with intensity inhomogenities. Based on clustering property of local intensity, to represent the image domain's partition and bias field that includes intensity inhomogenity, we defined energy of the level set functions. By minimizing the proposed energy functional, both segmentation and bias field estimation are jointly performed. The deviation property of bias field copied from the proposed energy is naturally protected by data term in deviational framework, without the demand to establish accurate smoothing term on the bias field. Compared

to piecewise smooth model, our method is more vigorous to initialization. Experimental results have determined preferable performance in terms of certainty, robustness and adaptability.

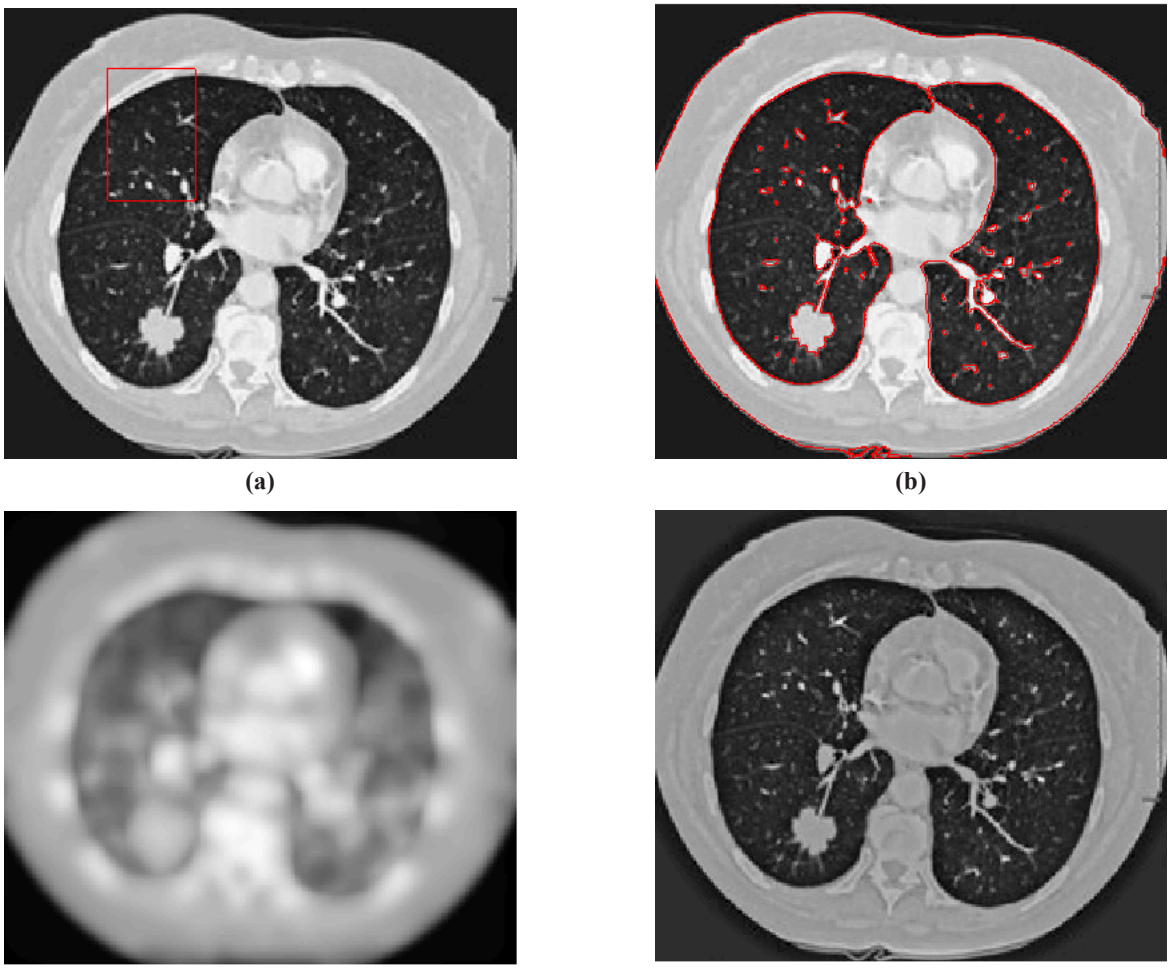

(a) **(b)**

(c) **(d)**

Figure 1: Application of our method to an MR image of lung.
(a) Original Image, (b) Segmented Image, (c) Estimated bias field, (d) Bias Corrected Image

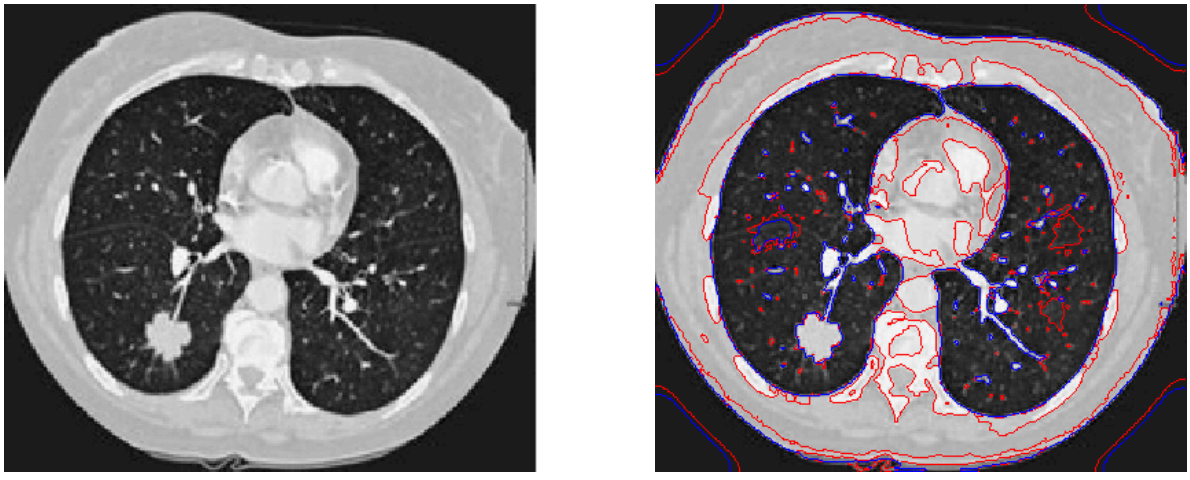

(a) **(b)**

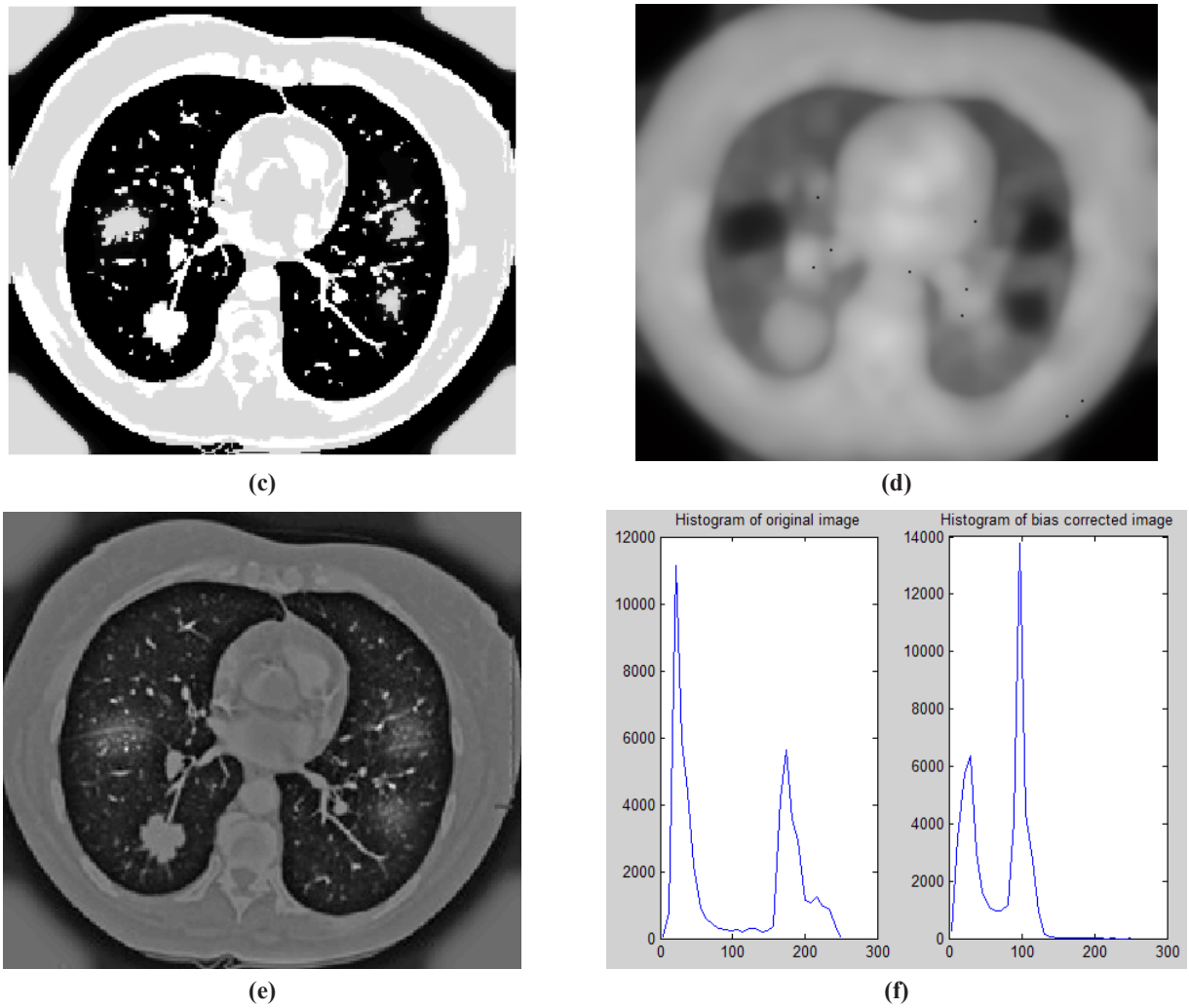

Figure 2: (a) Original image; (b): Final zero level contours of φ_1 (red) and φ_1 (blue), i.e. the segmentation result; (c): Segmented regions image (d): Estimated bias fields; (e): Bias corrected image; (f): Histograms of the original image and bias corrected images

REFERENCES

[1] T. Chan and L. Vese, "Active contours without edges", IEEE Trans. Image. Process, Vol. 10, No. 2, pp. 266-277, Feb. 2001.

[2] R. Ronfard, "Region-based strategies for active contour models," Int. J. Comput. Vis., Vol. 13, No. 2, pp. 229–251, Oct. 1994.

[3] C. Samson, L. Blanc-Feraud, G. Aubert, and J. Zerubia, "A variational model for image classification and restoration," IEEE Trans. Pattern Anal. Mach. Intell., Vol. 22, No. 5, pp. 460–472, May 2000.

[4] S.-C. Zhu and A. Yuille, "Region competition: Unifying snakes, region growing, and Bayes/MDL for multiband image segmentation," IEEE Trans. Pattern Anal. Mach. Intell., Vol. 18, No. 9, pp. 884–900, Sep. 1996.

[5] A. Vasilevskiy and K. Siddiqi, "Flux-maximizing geometric flows," IEEE Trans. Pattern Anal. Mach. Intell., Vol. 24, No. 12, pp. 1565–1578, Dec. 2002.

[6] V. Caselles, R. Kimmel, and G. Sapiro, "Geodesic active contours," Int. J. Comput. Vis., Vol. 22, No. 1, pp. 61–79, Feb. 1997.

[7] S. Kichenassamy, A. Kumar, P. Olver, A. Tannenbaum, and A. Yezzi, "Gradient flows and geometric active contour models," in Proc. 5th Int. Conf. Comput. Vis., 1995, pp. 810–815.

[8] N. Paragios and R. Deriche, "Geodesic active regions and level set methods for supervised texture segmentation," Int. J. Comput. Vis., Vol. 46, No. 3, pp. 223–247, Feb. 2002.

[9] Chunming Li, Rui Huang, Zhaohua Ding, J. Chris Gatenby, Dimitris N. Metaxas, Member, IEEE, and John C. Gore, "A Level Set Method for Image Segmentation in the Presence of Intensity Inhomogeneities With Application to MRI".

[10] C. Li, C. Kao, J. C. Gore, and Z. Ding, "Minimization of region-scalable fitting energy for image segmentation," IEEE Trans. Image Process., Vol. 17, No. 10, pp. 1940–1949, Oct. 2008.

[11] A. Tsai, A. Yezzi, and A. S.Willsky, "Curve evolution implementation of the Mumford-Shah functional for image segmentation, denoising, interpolation, and magnification," IEEE Trans. Image Process., Vol. 10, No. 8, pp. 1169–1186, Aug. 2001.

[12] R. Malladi, J. A. Sethian, and B. C.Vemuri, "Shape modeling with front propagation: A level set approach," IEEE Trans. Pattern Anal. Mach. Intell., Vol. 17, No. 2, pp. 158–175, Feb. 1995.

[13] R. Kimmel, A. Amir, and A. Bruckstein, "Finding shortest paths on surfaces using level set propagation," IEEE Trans. Pattern Anal. Mach. Intell., Vol. 17, No. 6, pp. 635–640, Jun. 1995.

[14] Ashis Kumar Dhara, Sudipta Mukhopadhyay, Satrajit Chakrabarty, Mandeep Garg, Niranjan Khandelwal, "Quantitative evaluation of margin sharpness of pulmonary nodules in lung CT images", IET Image Processing, Vol. 10, No. 9, pp. 631–637, 2016.

[15] J. H. S. Felix, P. C. Cortez, T. S. Cavalcante, A. R. Alexandria and M. A. Holanda, "AUTOIN: Method of Automatic Initialization of Active Contours Applied to Lungs in CT Images", IEEE Latin America Transactions, Vol. 10, No. 4, pp. 1954-1960, June. 2012.

[16] Panayiotis D. Korfiatis, Cristina Kalogeropoulou, Anna N. Karahaliou, Alexandra D. Kazantzi, and Lena I. Costaridou, "Vessel Tree Segmentation in Presence of Interstitial Lung Disease in MDCT", IEEE Transactions on Information Technology In Biomedicine, Vol. 15, No. 2, pp. 214-220, March 2011.

[17] Awais Mansoor, Ulas Bagci, Ziyue Xu, Brent Foster, Kenneth N. Olivier, Jason M. Elinoff, Anthony F. Suffredini, Jayaram K. Udupa, and Daniel J. Mollura, "A Generic Approach to Pathological Lung Segmentation", IEEE Transactions on Medical Imaging, Vol. 33, No. 12, pp. 2293-2310, Dec. 2014

[18] Y. Song, W. Cai, Y. Zhou, and D. Feng, "Feature-based image patch approximation for lung tissue classification," *IEEE Trans. Med. Imag.*, Vol. 32, No. 4, pp. 797–808, Apr. 2013.

[19] A. Mansoor, U. Bagci, and D. Mollura, "Near-optimal keypoint sampling for fast pathological lung segmentation," in *Proc. IEEE EMBC*, Chicago, IL, 2014, pp. 6032–6035.

[20] L. Wang, F. Shi, G. Li, Y. Gao, W. Lin, J. H. Gilmore, and D. Shen, "Segmentation of neonatal brain MR images using patch-driven level sets," *NeuroImage*, Vol. 84, pp. 141–158, 2014.

[21] N. Lay, N. Birkbeck, J. Zhang, and S. K. Zhou, "Rapidmulti-organ segmentation using context integration and discriminative models," *Inf. Process. Med. Imag.*, pp. 450–462, 2013.